# Fully Solution-Processed Semitransparent Organic Solar Cells with a Silver Nanowire Cathode and a Conducting Polymer Anode

**Jong Hyuk Yim,[†] Sung-yoon Joe,[†] Christina Pang,[‡] Kyung Moon Lee,[†] Huiseong Jeong,[†] Ji-Yong Park,[†] Yeong Hwan Ahn,[†] John C. de Mello,[‡,*] and Soonil Lee[†,*]**

[†]Department of Physics and Division of Energy Systems Research, Ajou University, Suwon 443-749, Korea and [‡]Centre for Plastic Electronics, Imperial College London, Exhibition Road, London SW7 2AZ, United Kingdom

**ABSTRACT** We report the fabrication of efficient indium–tin–oxide-free organic solar cells based on poly(3-hexylthiophene-2,5-diyl):[6,6]-phenyl-C61-butyric acid methyl ester (P3HT:PCBM). All layers of the devices from the lowermost silver nanowire cathode to the uppermost conducting polymer anode are deposited from solution and processed at plastic-compatible temperatures <200 °C. Owing to the absence of an opaque metal electrode, the devices are semitransparent with potential applications in power-generating windows and tandem-cells. The measured power conversion efficiencies (PCEs) of 2.3 and 2.0% under cathode- and anode-side illumination, respectively, match previously reported PCE values for equivalent semitransparent organic solar cells using indium tin oxide.

**KEYWORDS:** transparent conducting electrode · silver nanowire · conducting polymer · full solution processability · semitransparent organic solar cell

Transparent conducting electrodes (TCEs), which make electrical contact to other functional layers for current supply/extraction while also transmitting light, are essential components of optoelectronic devices. State-of-the-art TCEs are made of metal oxides, most commonly indium tin oxide (ITO) which has a typical sheet resistance ($R_{sq}$) of ~10 Ω sq$^{-1}$ at 90% transparency.[1] ITO, however, suffers from several drawbacks that limit its viability as a TCE for next-generation optoelectronics, including high cost, poor performance on plastic substrates, and a tendency to crack when flexed.[2,3]

Potential solution-processable alternatives to ITO include carbon nanotubes,[4,5] graphene,[6−9] conducting polymers,[10,11] and metal nanowires[12−15] Single-Walled Carbon Nanotubes (SWCNTs) are attractive TCE materials due to their high intrinsic conductivity and mechanical durability but, owing to large intertube resistances, their reported performance characteristics are significantly worse than ITO. The need for aggressive acid treatments to induce p-type doping of semiconducting tubes and the nonpermanent nature of the doped state are also problematic.[16] Graphene is another potential TCE material among the carbon allotropes, with Bae *et al.* having reported 30-in. graphene films with sheet resistances of 30 Ω sq$^{-1}$ at transmittances of ~90%.[9] The fabrication procedure however involved a combination of chemical vapor deposition (CVD), chemical etching, and solid-state transfer, and is unlikely to transfer easily to large-scale industrial use. Graphene TCEs may alternatively be prepared from a dispersion of graphene oxide,[6,7] which can be cast onto a substrate and then reduced to render it conductive. The reduction step, however, requires high temperatures and/or harsh reagents such as hydrazine and is consequently ill-suited to direct deposition on plastic substrates. Moreover, the resultant films show sheet-resistances that are more than ten times higher than CVD-graphene.

* Address correspondence to soonil@ajou.ac.kr, j.demello@imperial.ac.uk.

Received for review December 31, 2013 and accepted February 8, 2014.

**Published online February 17, 2014**
**10.1021/nn406672n**

Modification of poly(3,4-ethylenedioxythiophene): poly(styrenesulfonate) (PEDOT:PSS) is a promising approach to high performance polymeric TCEs.[11,17] PEDOT:PSS, doped with dimethylsulfoxide (DMSO) and Zonyl FS-300 fluorinated surfactant, can yield TCEs with transmittances >90% at sheet resistances <100 Ω $sq^{-1}$. Kaltenbrunner *et al.* reported that the power conversion efficiencies (PCEs) of poly(3-hexylthiophene-2,5-diyl):[6,6]-phenyl-C61-butyric acid methyl ester (P3HT:PCBM) organic solar cells (OSCs) using highly conductive PEDOT:PSS on plastic were comparable to equivalent devices using ITO-coated glass.[17] They further demonstrated that PEDOT:PSS-based devices were more mechanically resilient than equivalent ITO-based devices on plastic, suffering only slight reductions in performance under repeated flexing.

Recently, TCEs based on silver nanowires (AgNWs) have been shown to provide high flexibility, while providing transmittances and sheet-resistances at the level of ITO.[14,18−20] Several groups have tested solution-deposited AgNW films in OSCs, using them as a bottom or a top electrode, and frequently achieving comparable PCEs to equivalent ITO-based devices.[21−27] Virtually all devices reported to date, however, have used ITO or a thermally evaporated metal as the counter electrode, with a consequent need for vacuum processing during fabrication. The development of fully solution-processed devices, fabricated at plastic-compatible temperatures, would greatly enhance the industrial viability of OSC technology.

To achieve full solution processability, several technical challenges must be addressed. Interfaces must be engineered to give Ohmic contacts at the cathode and anode for efficient electron and hole collection, respectively. At the same time, both interfaces must be selective with respect to charge transport, passing only the desired charge carrier while blocking the other carrier type. Moreover, all constituent layers should be smooth, and energetically matched to (and chemically compatible with) adjacent layers so that a multilayered device with well-defined interfaces can be produced. Satisfying these requirements with low temperature, solution-processed materials is challenging, especially when nonuniform TCEs such as AgNWs are used.

Here we report the use of AgNWs (Cambrios ClearOhm) and highly doped PEDOT:PSS (Clevios PH 1000) as solution-processed cathode and anode materials in inverted P3HT:PCBM bulk heterojunction (BHJ) OSCs. Both electrodes, together with all other (charge-generating and charge-transporting) layers in the device, are deposited from solution under ambient conditions and processed at plastic compatible temperatures. The resultant devices, which use no opaque metals, are semitransparent and exhibit favorably high PCEs of 2.3 and 2.0% for cathode and anode side illumination, respectively. Despite their fully solution-processed nature, they are comparable in efficiency to previously reported semitransparent OSCs with ITO, which have been reported to have PCEs in the range 1.9−2.5%.[27−31] The efficiencies also compare well with a very recent report by Guo *et al.*[32] where PCEs of 2.3% were achieved using AgNWs for both electrodes (although, in contrast to the devices described here, a ternary-blend of P3HT, PCBM and the low band gap polymer poly-[(4,40-bis(2-ethylhexyl)-dithieno[3,2-*b*:20,30-*d*]silole)-2,6-diyl-*alt*-(2,1,3-benzothiadia-zole)-4,7-diyl] (Si-PCPDTBT) was employed as the active layer).

## RESULTS AND DISCUSSION

The transmittance *versus* sheet-resistance trade-off characteristics of TCEs are commonly quantified in terms of the ratio $\sigma_{dc}/\sigma_{op}$ in the Tinkham formula:[16]

$$T(\lambda) = \left(1 + \frac{Z_0}{2R_{sq}}\frac{\sigma_{op}(\lambda)}{\sigma_{dc}}\right)^{-2} \quad (1)$$

This equation describes the relationship between optical transmittance $T$ and sheet resistance $R_{sq}$ for a thin conducting film, with $Z_0$ being the free space impedance (377 Ω), $\lambda$ the wavelength of transmitted light, and $\sigma_{op}$ and $\sigma_{dc}$ the film's optical and DC conductivities. Higher values of $\sigma_{dc}/\sigma_{op}$ indicate higher transmittance for a given sheet-resistance, and $\sigma_{dc}/\sigma_{op}$ must typically be >35 for practical device applications.[10] Figure 1 shows the 550 nm trade-off characteristics for AgNW and PH 1000 TCEs of varying thickness. The values of $\sigma_{dc}/\sigma_{op}$ deduced from the best-fit curves in Figure 1a,c are 360 ± 30 for the AgNWs and 50 ± 1.5 for PH 1000. The AgNW value is fairly close to that of ITO ($\sigma_{dc}/\sigma_{op} \sim 500$) and an order of magnitude higher than for SWCNTs ($\sigma_{dc}/\sigma_{op} \sim 24$),[5] graphene ($\sigma_{dc}/\sigma_{op} \sim 70$),[9] and PH 1000 ($\sigma_{dc}/\sigma_{op} \sim 50$).[11] A similar $\sigma_{dc}/\sigma_{op}$ value has previously been reported for AgNW films, but over a limited transmittance range ($T < 80\%$).[33] In the case of PH 1000 films modified with 5 vol % DMSO and 0.5% Zonyl FS-300 fluorosurfactant (see Experimental Section), the deduced $\sigma_{dc}/\sigma_{op}$ value agrees closely with that reported by Vosgueritchian *et al.*[11]

A characteristic feature of AgNW films is significant haziness due to scattering of visible light. To quantify the haze of our AgNW films, we measured their total transmittance with an integrating sphere, collecting all forward-scattered light. In all cases, the total transmittance was measurably larger than the specular transmittance, with the difference ($\Delta T\%$) being greatest for the thickest (lowest $R_{sq}$) films (Figure 1d). AgNWs are a few tens of nanometres in diameter and, as progressively more nanowires are deposited to reduce sheet resistance, they overlap to form geometrical features with heights or lateral sizes that are of order a few hundreds of nanometres and consequently scatter visible light strongly. (Light scattering by individual

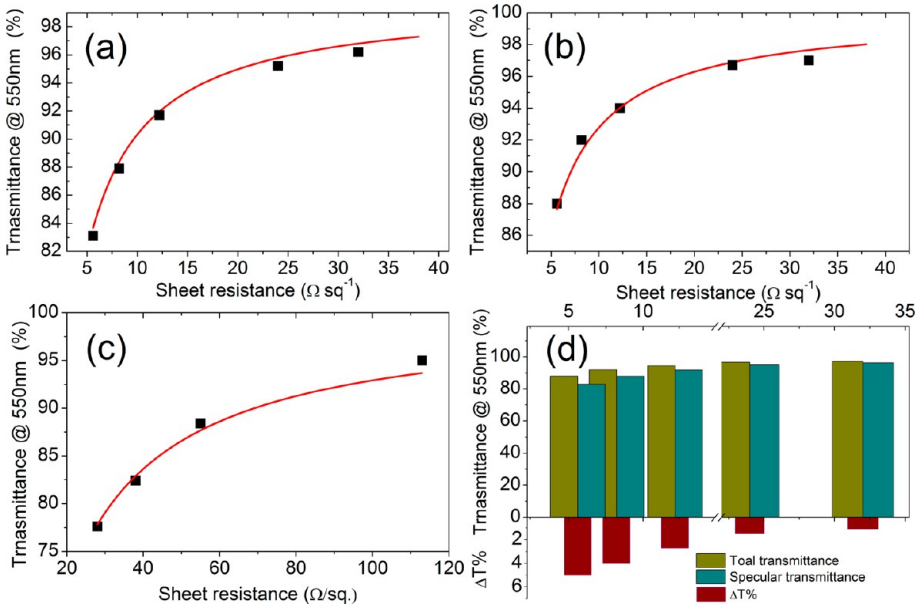


**Figure 1. Optical transmittance ($\lambda$ = 550 nm) *versus* sheet resistance for AgNW and PH 1000 transparent conducting electrodes for: (a) AgNWs in specular transmittance, (b) AgNWs in total transmittance, and (c) PH1000 in specular transmittance. Square markers are experimental data, and solid lines denote numerical fits to Tinkham's formula. (d) Bar graph showing how the difference between the specular and total transmittance of the AgNW electrodes varies with sheet resistance. A blank glass substrate was used as a reference for the transmittance measurements.**

AgNWs can also cause haziness, but this effect dominates for thin films). While haze is undesirable for display applications, forward scattering of incident light can be advantageous for solar cells where it can increase path-lengths in the active layer and hence enhance photon capture. Strikingly, when the total transmittance *versus* sheet resistance characteristics were fitted to eq 1 (Figure 1b), the inferred $\sigma_{dc}/\sigma_{op}$ value of 493 $\pm$ 42 was very close to that of device-grade ITO (~500), implying the efficiencies of AgNW-based OSCs should match conventional ITO-based devices.

For the devices reported here, AgNWs were used as the bottom electrode to allow photolithographic patterning (see Experimental Section and Supporting Information, Figure S1 and Figure S2) and to minimize the risk of air-oxidation, while PH 1000 was used for the top electrode because it is air-stable and can be readily patterned using a shadow mask or contact-printing. One advantage of this configuration is that the higher transmittance of the AgNWs partially offsets optical losses in the glass substrate, and so allows comparable transmittances to be achieved for illumination *via* the glass/AgNW and PH 1000 windows.

Compared to most other TCEs, AgNW films are very rough due to their random-network morphology and the tens of nanometer diameters of individual nanowires. Figure 2a shows a typical atomic force microscopy (AFM) image of an as-coated $R_{sq}$ = 13 Ω sq$^{-1}$ AgNW film on glass. The root-mean-square (RMS) roughness of the film estimated from the 15 × 15 $\mu$m$^2$ scan image is 18 nm, while the peak-to-valley height is ~125 nm. Such high roughness is problematic for organic device fabrication due to the significant risk of shorting through other layers in the stack. Hence, as previously described by Leem *et al.*,[23] the roughness was reduced by modifying the surface of the AgNWs with n-type metal oxides, a combination of ultrathin $TiO_x$ and thick ZnO (nominal thickness ~40 nm). The latter was selected as an electron transport material (ETM) due to its excellent transparency, environmental stability and high electron mobility, with the $TiO_x$ precoating being required to ensure reliable coating of the sol–gel ZnO layer, and to improve the adhesion of the AgNW film to the glass substrates. Strong adhesion is essential for maintaining the integrity of the AgNW electrode throughout the solution processes used to deposit subsequent layers. (Note, $TiO_x$ was not used as the ETM since the chosen Tyzor precursor must be annealed above 400 °C to attain adequate electron mobilities.) An AFM image of a 13 Ω sq$^{-1}$ AgNW film coated with $TiO_x$/ZnO is shown in Figure 2b. The RMS roughness and peak-to-valley height have been greatly reduced to 10 and 75 nm, respectively, due to the small ZnO grains covering exposed regions of the substrate and filling voids between nanowires. Importantly, the oxide-coated AgNWs presented no difficulties in fabricating OSCs with a 210 nm P3HT:PCBM active layer.

Figure 3 shows current density *versus* voltage ($J$–$V$) characteristics for two control devices of area 0.24 cm$^2$ (Supporting Information, Figure S2), each having a ~17 Ω sq$^{-1}$ AgNW cathode at the bottom and an evaporated Ag (E-Ag) anode on top. For the first control device, a 210 nm layer of P3HT:PCBM was

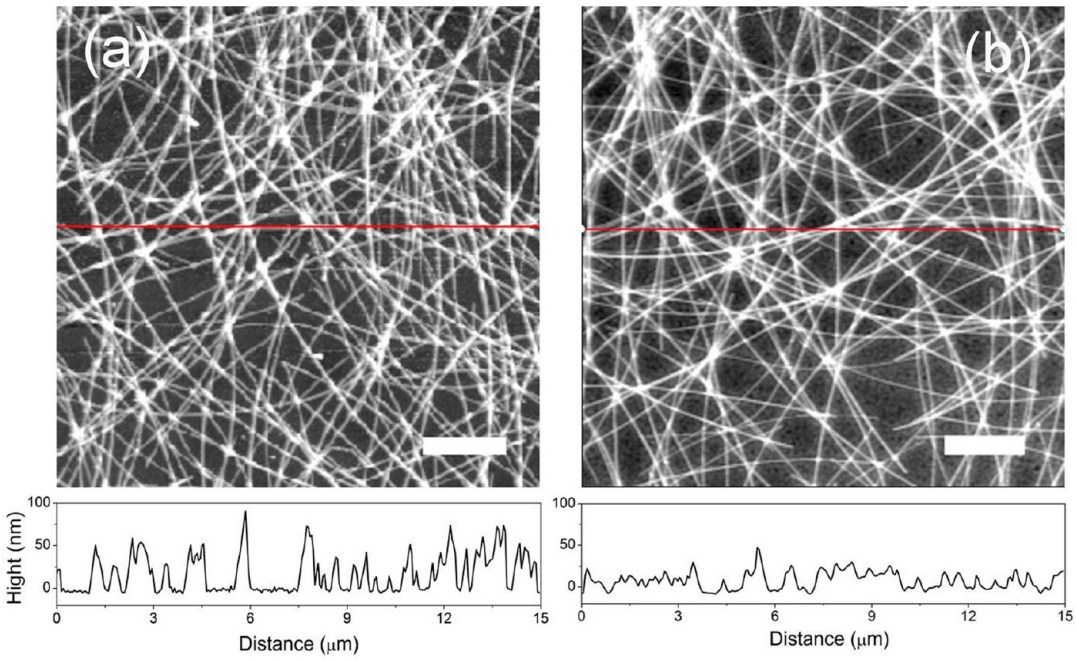


**Figure 2. Typical AFM images of (a) as-deposited and (b) $TiO_x$/ZnO-modified AgNW films. Scale bar is 2.5 $\mu$m. Line profiles along the red lines are shown below the respective AFM images.**

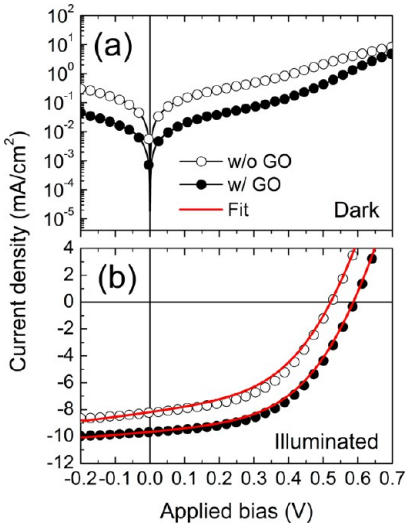


**Figure 3. $J-V$ characteristics of the control devices with and without a layer of graphene oxide in between the Al 4083 and the E−Ag anode: (a) in the dark and (b) under AM 1.5 solar illumination. The control devices have an AgNW cathode at the bottom and a reflective Ag anode at the top. Red solid lines are best-fit curves to a nonideal diode model.**

deposited on the oxide-coated AgNWs, followed by a 30 nm layer of low conductivity PEDOT:PSS (Clevios Al 4083), and then the E-Ag anode. The device had a short-circuit current ($J_{sc}$) of 8.2 mA cm$^{-2}$, an open-circuit voltage ($V_{oc}$) of 0.52 V, and a fill factor (FF) of 49% under AM 1.5 solar illumination at 1 sun, resulting in a modest PCE of 2.1%. It is common to model the operation of OSCs as nonideal diodes. The equivalent circuit parameters, obtained by fitting the $J-V$ curve in Figure 3b to the diode equation with parasitic resistances, were 3.7, 7.0, and 302 Ω cm$^2$ for the ideality factor ($n$), the series resistance ($R_S$), and the shunt ($R_{SH}$) resistances, respectively. The shunt resistance corresponding to the dark $J-V$ curve in Figure 3a was 15 kΩ cm$^2$. The values of the ideality factor and series resistance are comparable to those of typical ITO-based devices with E-Ag top electrodes, but the shunt resistance is rather low and is the principal reason for the small $V_{oc}$ and relatively low PCE.

In practice, it is difficult to deposit aqueous Al 4083 solution onto hydrophobic P3HT:PCBM. Despite adding Zonyl surfactant to reduce its surface tension, the Al 4083 solution wetted the P3HT:PCBM layer poorly, and many devices suffered from large leakage currents or electrical shorts due to pinholes and nonuniform topography. To remedy this problem, in our second control device, we incorporated a thin (2−3 nm) solution-deposited layer of graphene oxide between the Al 4083 and the E−Ag anode which, despite its ultrathin nature, resulted in much better performance. The GO-containing device had a $J_{sc}$ of 9.7 mA cm$^{-2}$, a $V_{oc}$ of 0.59 V, and a FF of 51% under AM 1.5 solar illumination at 1 sun, corresponding to an enhanced PCE of 2.9%. Fitting the $J-V$ curve in Figure 3b to the nonideal diode equation revealed substantially improved diode parameters of $n$ = 3.8, $R_S$ = 6.7 Ω cm$^2$, and $R_{SH}$ = 478 Ω cm$^2$ under illumination, while $R_{SH}$ corresponding to the dark $J-V$ curve in Figure 3a was ∼158 kΩ cm$^2$. The slight reduction in $R_S$ and substantial increase in $R_{SH}$ indicate improved contact selectivity with the GO layer present, suggesting an improved contact and reduced recombination currents at the E−Ag anode (attributable to the

suppression of electron back flows). This in turn produces higher $J_{sc}$ and FF values, resulting in lower reverse currents and larger $V_{oc}$.

The deposition of GO on the Al 4083 layer induced only minor topographical changes. Before coating, the Al 4083 had a granular surface (Figure 4a) with an RMS roughness of 7.8 nm. Deposition of the GO layer resulted in only a slight reduction in the RMS roughness to 6.6 nm, with the granular surface-structure remaining largely unchanged (Figure 4b). We conclude that the GO conformally coats the irregular Al 4083 surface, covering pinholes and making the surface more chemically and electronically uniform. This in turn allows a better contact to be formed with the E−Ag anode.

For OSCs with a spin-coated PH 1000 anode (instead of E−Ag), the GO layer served an additional critical function. Uneven coating of PH 1000 on the hydrophobic Al 4083 was a frequent cause of device failure, resulting in device yields of <50% (7 out of 16). Inclusion of the (hydrophilic) GO layer led to improved wetting of the PH 1000 dispersion and protected the underlying multilayer structure from damage by strong capillary forces during spin-coating and drying, thereby increasing yields to ~85% (21 out of 24).

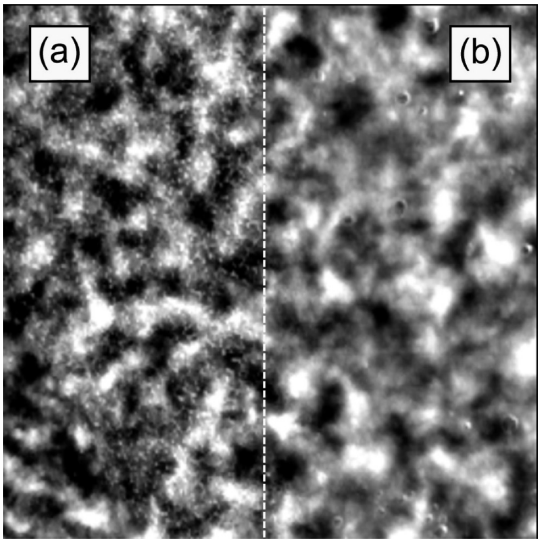


**Figure 4. Topography images of Al 4083 on P3HT:PCBM without (a) and with (b) a coating of graphene oxide. The 15 × 15 $\mu$m$^2$ images were scanned in the *x*-axis direction. The additional GO layer caused only a slight reduction in RMS surface roughness from 7.8 nm (Al 4083 on P3HT:PCBM) to 6.6 nm (GO on Al4083 on P3HT:PCBM).**

The devices displayed ~55% transparency at long wavelengths beyond 650 nm (Figure 5a), where the P3HT:PCBM active layer is largely absorption-free, opening up potential applications in, *e.g.*, power-generating windows and tandem-cell devices. Figure 5b compares the $J-V$ characteristics under illumination through the AgNW cathode and through the PH 1000 anode (AM 1.5, 1 sun conditions). When illuminated through the cathode the device showed $R_S$ = 7.9 Ω cm$^2$, $R_{SH}$ = 351 Ω cm$^2$, $J_{sc}$ = 8.2 mA cm$^{-2}$, $V_{oc}$ = 0.58 V and FF = 49%, corresponding to a PCE of 2.3%. The main difference between the (GO-containing) E−Ag control device (which had a PCE of 2.9%) and the semitransparent device under cathode-side illumination is the lower $J_{sc}$ of the latter, which we attribute to reduced light absorption in the P3HT:PCBM active layer. Unlike the control device, with its mirror-like top electrode, there is minimal reflection at the GO/PH 1000 interface and so negligible enhancement in the path-length through the active layer. Additionally, the slight increase in $R_S$ and decrease in $R_{SH}$ relative to the control device can be attributed to the higher sheet resistance of PH 1000 and a slightly lower quality anodic junction between the GO-covered Al 4083 and PH 1000 compared to E−Ag. When illuminated through the PH 1000, the semitransparent device showed slightly worse performance with $R_S$ = 12.6 Ω cm$^2$, $R_{SH}$ = 707 Ω cm$^2$, $J_{sc}$ = 7.1 mA cm$^{-2}$, $V_{oc}$ = 0.58 V, and FF = 49%, corresponding to a PCE of 2.0%. Hence the $V_{oc}$ and FF values were equal for the two illumination directions, whereas the $J_{sc}$ and $R_S$ values differed.

Transmittance differences between the cathode and anode windows are not sufficient to explain the dependence of $J_{sc}$ on illumination direction. The cathode window (Glass/AgNWs/ZnO) and the anode window (PH 1000/GO/Al 4083) had similar average transmittances of 84 and 83% between 450 and 650 nm, *i.e.*, across the absorbing region of P3HT (Supporting Information, Figure S3). However, significant differences were observed in the external quantum efficiency

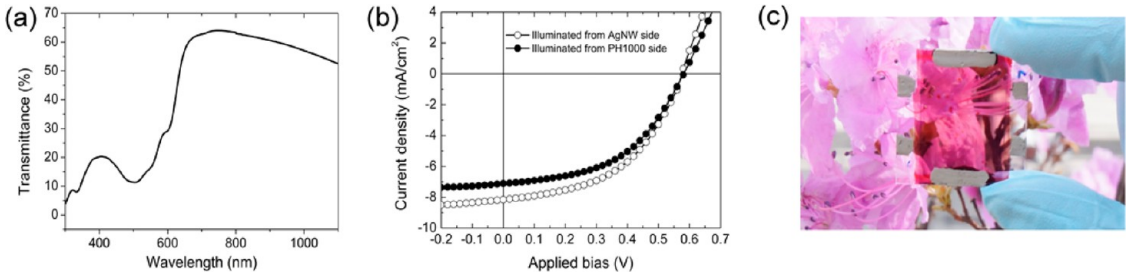


**Figure 5. (a) The optical transmittance spectrum of a typical semitransparent P3HT:PCBM solar cell with AgNW- and PH1000-based TCEs. (b) $J-V$ characteristics of the semitransparent P3HT:PCBM solar cell illuminated through the AgNW and the PH1000 electrodes. (c) A photograph of a typical semitransparent P3HT:PCBM solar cell.**

(EQE) spectra. The largest discrepancy occurred at 530 nm, near the EQE peak for cathode-side illumination (Supporting Information, Figure S4). Given the similarity of the solar photon absorption spectra for the two illumination directions (Supporting Information, Figure S5) and the monotonic decrease in the exciton-generation rates with distance into the P3HT:PCBM layer (Supporting Information, Figure S6), we attribute the different $J_{sc}$ values to differences in the likelihood of an exciton reaching a dissociation site. The observed behavior is consistent with the P3HT−PCBM interfaces being located asymmetrically with respect to the two electrodes, with the majority of P3HT−PCBM junctions lying closer to the AgNW cathode and hence yielding higher photocurrents under cathode-side illumination (see Supporting Information for detailed discussion).

## CONCLUSIONS

In conclusion, AgNW and PH 1000 TCEs both satisfy baseline industry targets of $\sigma_{dc}/\sigma_{op} > 35$, and could potentially replace ITO in selected optoelectronic devices. Indeed, taking forward-light-scattering into account, we found AgNWs to have a $\sigma_{dc}/\sigma_{op}$ value of 493 ± 42, close to the best device-grade ITO. Using these two electrodes in combination, we have fabricated fully solution-processed semitransparent P3HT:PCBM BHJ OSCs in an inverted configuration with a lower AgNW cathode and an upper PH 1000 anode. $TiO_x$/ZnO and Al4083/GO were selected as respective cathode and anode buffer layers to achieve high PCEs, improve fabrication yields, and balance the influx of solar spectrum photons to the P3HT:PCBM active layer for the two illumination directions. The fully solution-processed semitransparent OSCs, which were produced under ambient conditions at plastic-compatible temperatures <200 °C, had PCEs of 2.3 and 2.0% under cathode- and anode-side illumination, respectively. The devices are comparable in efficiency to previously reported semitransparent devices using ITO bottom electrodes and P3HT:PCBM active layers.[27−31] They also match the 2.3% efficiency of a recently reported fully solution-processed semitransparent device using AgNWs as both the bottom and top electrodes and a ternary blend of P3HT, Si-PCPDTBT and PCBM as the active layer.[32] Further improvements in PCE can be expected with the adoption of lower band gap donors, alternative fullerene acceptors, photonic structures to enhance light collection or tandem-cell architectures to harvest infrared-photons.

## EXPERIMENTAL SECTION

AgNW films of varying surface coverage were spin-coated onto clean (3-aminopropyl)triethoxysilane treated 3 × 3 $cm^2$ glass substrates from as-received Cambrios ClearOhm AgNW dispersion, using speeds between 500 and 4000 rpm. After drying for 1 min at 60 °C and annealing at 140 °C for 30 min, TCEs with sheet resistances from 5 to 35 Ω $sq^{-1}$ were obtained (as determined by four-point-probe testing). The films were characterized using a UV−vis spectrophotometer (Cary 5000, Varian), and an Atomic Force Microscope (XE-100, Park system).

To fabricate devices, 13−18 Ω $sq^{-1}$AgNW films on 3 × 3 $cm^2$ glass substrates were photolithographically patterned into the desired electrode shape, either a strip for the control devices or a finger pattern for the semitransparent devices (see Supporting Information, Figure S2). $TiO_x$ surface layers were deposited on the patterned AgNW films by spin-coating a 0.1 wt % ethanolic solution of Tyzor, and then annealing at 120 °C for 30 min. Sol−gel ZnO layers were spin-coated on the $TiO_x$ from a precursor formulation proposed by Sun *et al.*[34] and then baked at 200 °C for 1 h. The nominal thickness of the ZnO layers, *i.e.*, the thickness when deposited under identical conditions on a smooth glass substrate, was ∼40 nm. A dichlorobenzene solution containing a 40 mg $mL^{-1}$ 1:1 mixture of P3HT and PCBM was spin-coated onto the ZnO, yielding a ∼210 nm film, and then baked at 140 °C for 10 min. Filtered and ultrasonicated PEDOT:PSS (Clevios P VP Al 4083) mixed with 1 vol % Zonyl surfactant (FSO-100) was spin-coated onto the active layer at 5000 rpm for 1 min, before baking at 110 °C for 10 min. Aqueous graphene oxide (0.5 mg $mL^{-1}$ ) was prepared from purified graphite by a modification of Hummer's method[35] and mixed with 0.5 vol % Zonyl surfactant. An optional GO layer was spin-coated onto the Al 4083 at 5000 rpm for 1 min and then baked at 110 °C for 10 min. Devices were completed by twice spin-coating Clevios PH 1000 PEDOT:PSS mixed with 5 vol % DMSO and 0.5 vol % Zonyl (FS-300) onto the uppermost surface at 1000 rpm for 90 s, masking the surface with removable tape to define the anode area, and then baking at 120 °C for 5 min. The resultant ∼250 nm anode had a sheet resistance of ∼55 Ω $sq^{-1}$. For the control devices, an 80 nm Ag anode was evaporated through a shadow mask at 2 × $10^{-6}$ Torr. The pixel size, defined by the overlap of cathode and anode, was 0.24 $cm^2$ in all cases. Devices were tested under AM 1.5G illumination at 1 sun, using an Abet LS 150 Xe arc lamp source with an appropriate filter.

*Conflict of Interest:* The authors declare no competing financial interest.

*Acknowledgment.* This research was supported by the Basic Science Research Program through the National Research Foundation of Korea (NRF) funded by the Ministry of Education (NRF-2009-0094046), and by the Program for International Cooperative R&D between Industry, Academy, and Research Institute (SMBA Grant No. 00035633) funded by the Korea Small and Medium Business Administration. ClearOhm AgNW dispersion was kindly supplied by Cambrios.

*Supporting Information Available:* Schematics of the device architectures and the electrode patterns, and a discussion of the influence of illumination direction on the EQE. This material is available free of charge *via* the Internet at http://pubs.acs.org.

## REFERENCES AND NOTES

1. Bel Hadj Tahar, R.; Ban, T.; Ohya, Y.; Takahashi, Y. Tin Doped Indium Oxide Thin Films: Electrical Properties. *J. Appl. Phys.* **1998**, *83*, 2631.
2. Chen, Z.; Cotterell, B.; Wang, W.; Guenther, E.; Chua, S.-J. A Mechanical Assessment of Flexible Optoelectronic Devices. *Thin Solid Films* **2001**, *394*, 201–205.
3. Kim, H.-K.; Kim, D.-G.; Lee, K.-S.; Huh, M.-S.; Jeong, S. H.; Kim, K. I.; Seong, T.-Y. Plasma Damage-Free Sputtering of Indium Tin Oxide Cathode Layers for Top-Emitting Organic Light-Emitting Diodes. *Appl. Phys. Lett.* **2005**, *86*, 183503.
4. Chandra, B.; Afzali, A.; Khare, N.; El-Ashry, M. M.; Tulevski, G. S. Stable Charge-Transfer Doping of Transparent

Single-Walled Carbon Nanotube Films. *Chem. Mater.* **2010**, *22*, 5179–5183.
5. Hellstrom, S. L.; Vosgueritchian, M.; Stoltenberg, R. M.; Irfan, I.; Hammock, M.; Wang, Y. B.; Jia, C.; Guo, X.; Gao, Y.; Bao, Z. Strong and Stable Doping of Carbon Nanotubes and Graphene by MoOx for Transparent Electrodes. *Nano Lett.* **2012**, *12*, 3574–3580.
6. Pei, S.; Zhao, J.; Du, J.; Ren, W.; Cheng, H.-M. Direct Reduction of Graphene Oxide Films into Highly Conductive and Flexible Graphene Films by Hydrohalic Acids. *Carbon* **2010**, *48*, 4466–4474.
7. Becerril, H. A.; Mao, J.; Liu, Z.; Stoltenberg, R. M.; Bao, Z.; Chen, Y. Evaluation of Solution-Processed Reduced Graphene Oxide Films as Transparent Conductors. *ACS Nano* **2008**, *2*, 463–470.
8. Li, X.; Zhu, Y.; Cai, W.; Borysiak, M.; Han, B.; Chen, D.; Piner, R. D.; Colombo, L.; Ruoff, R. S. Transfer of Large-Area Graphene Films for High-Performance Transparent Conductive Electrodes. *Nano Lett.* **2009**, *9*, 4359–4363.
9. Bae, S.; Kim, H.; Lee, Y.; Xu, X.; Park, J.-S.; Zheng, Y.; Balakrishnan, J.; Lei, T.; Kim, H. R.; Song, Y. I.; *et al.* Roll-to-Roll Production of 30-Inch Graphene Films for Transparent Electrodes. *Nat. Nanotechnol.* **2010**, *5*, 574–578.
10. Alemu, D.; Wei, H.-Y.; Ho, K.-C.; Chu, C.-W. Highly Conductive PEDOT:PSS Electrode by Simple Film Treatment with Methanol for ITO-Free Polymer Solar Cells. *Energy Environ. Sci.* **2012**, *5*, 9662.
11. Vosgueritchian, M.; Lipomi, D. J.; Bao, Z. Highly Conductive and Transparent PEDOT:PSS Films with a Fluorosurfactant for Stretchable and Flexible Transparent Electrodes. *Adv. Funct. Mater.* **2012**, *22*, 421–428.
12. Zhang, D.; Wang, R.; Wen, M.; Weng, D.; Cui, X.; Sun, J.; Li, H.; Lu, Y. Synthesis of Ultralong Copper Nanowires for High-Performance Transparent Electrodes. *J. Am. Chem. Soc.* **2012**, *134*, 14283–14286.
13. Azulai, D.; Belenkova, T.; Gilon, H.; Barkay, Z.; Markovich, G. Transparent Metal Nanowire Thin Films Prepared in Mesostructured Templates. *Nano Lett.* **2009**, *9*, 4246–4249.
14. Hu, L.; Kim, H. S.; Lee, J.-Y.; Peumans, P.; Cui, Y. Scalable Coating and Properties of Transparent, Flexible, Silver Nanowire Electrodes. *ACS Nano* **2010**, *4*, 2955–2963.
15. Liu, C.-H.; Yu, X. Silver Nanowire-Based Transparent, Flexible, and Conductive Thin Film. *Nanoscale Res. Lett.* **2011**, *6*, 75.
16. Hecht, D. S.; Hu, L.; Irvin, G. Emerging Transparent Electrodes Based on Thin Films of Carbon Nanotubes, Graphene, and Metallic Nanostructures. *Adv. Mater.* **2011**, *23*, 1482–1513.
17. Kaltenbrunner, M.; White, M. S.; Głowacki, E. D.; Sekitani, T.; Someya, T.; Sariciftci, N. S.; Bauer, S. Ultrathin and Lightweight Organic Solar Cells with High Flexibility. *Nat. Commun.* **2012**, *3*, 770.
18. Bergin, S. M.; Chen, Y.-H.; Rathmell, A. R.; Charbonneau, P.; Li, Z.-Y.; Wiley, B. J. The Effect of Nanowire Length and Diameter on the Properties of Transparent, Conducting Nanowire Films. *Nanoscale* **2012**, *4*, 1996–2004.
19. Lee, J.-Y.; Connor, S. T.; Cui, Y.; Peumans, P. Solution-Processed Metal Nanowire Mesh Transparent Electrodes. *Nano Lett.* **2008**, *8*, 689–692.
20. Zeng, X.-Y.; Zhang, Q.-K.; Yu, R.-M.; Lu, C.-Z. A New Transparent Conductor: Silver Nanowire Film Buried at the Surface of a Transparent Polymer. *Adv. Mater.* **2010**, *22*, 4484–4488.
21. Gaynor, W.; Lee, J.-Y.; Peumans, P. Fully Solution-Processed Inverted Polymer Solar Cells with Laminated Nanowire Electrodes. *ACS Nano* **2010**, *4*, 30–34.
22. Lee, J.-Y.; Connor, S. T.; Cui, Y.; Peumans, P. Semitransparent Organic Photovoltaic Cells with Laminated Top Electrode. *Nano Lett.* **2010**, *10*, 1276–1279.
23. Leem, D.-S.; Edwards, A.; Faist, M.; Nelson, J.; Bradley, D. D. C.; de Mello, J. C. Efficient Organic Solar Cells with Solution-Processed Silver Nanowire Electrodes. *Adv. Mater.* **2011**, *23*, 4371–4375.
24. Yang, L.; Zhang, T.; Zhou, H.; Price, S. C.; Wiley, B. J.; You, W. Solution-Processed Flexible Polymer Solar Cells with Silver Nanowire Electrodes. *ACS Appl. Mater. Interfaces* **2011**, *3*, 4075–4084.
25. Zhu, R.; Chung, C.-H.; Cha, K. C.; Yang, W.; Zheng, Y. B.; Zhou, H.; Song, T.-B.; Chen, C.-C.; Weiss, P. S.; Li, G.; *et al.* Fused Silver Nanowires with Metal Oxide Nanoparticles and Organic Polymers for Highly Transparent Conductors. *ACS Nano* **2011**, *5*, 9877–9882.
26. Chen, C.-C.; Dou, L.; Zhu, R.; Chung, C.-H.; Song, T.-B.; Zheng, Y. B.; Hawks, S.; Li, G.; Weiss, P. S.; Yang, Y. Visibly Transparent Polymer Solar Cells Produced by Solution Processing. *ACS Nano* **2012**, *6*, 7185–7190.
27. Krantz, J.; Stubhan, T.; Richter, M.; Spallek, S.; Litzov, I.; Matt, G. J.; Spiecker, E.; Brabec, C. J. Spray-Coated Silver Nanowires as Top Electrode Layer in Semitransparent P3HT:PCBM-Based Organic Solar Cell Devices. *Adv. Funct. Mater.* **2013**, *23*, 1711–1717.
28. Lee, Y.-Y.; Tu, K.-H.; Yu, C.-C.; Li, S.-S.; Hwang, J.-Y.; Lin, C.-C.; Chen, K.-H.; Chen, L.-C.; Chen, H.-L.; Chen, C.-W. Top Laminated Graphene Electrode in a Semitransparent Polymer Solar Cell by Simultaneous Thermal Annealing/Releasing Method. *ACS Nano* **2011**, *5*, 6564–6570.
29. Hau, S. K.; Yip, H.-L.; Zou, J.; Jen, A. K.-Y. Indium Tin Oxide-Free Semi-Transparent Inverted Polymer Solar Cells Using Conducting Polymer as Both Bottom and Top Electrodes. *Org. Electron.* **2009**, *10*, 1401–1407.
30. Schmidt, H.; Flügge, H.; Winkler, T.; Bülow, T.; Riedl, T.; Kowalsky, W. Efficient Semitransparent Inverted Organic Solar Cells with Indium Tin Oxide Top Electrode. *Appl. Phys. Lett.* **2009**, *94*, 243302.
31. Colsmann, A.; Reinhard, M.; Kwon, T.-H.; Kayser, C.; Nickel, F.; Czolk, J.; Lemmer, U.; Clark, N.; Jasieniak, J.; Holmes, A. B.; *et al.* Inverted Semi-Transparent Organic Solar Cells with Spray Coated, Surfactant Free Polymer Top-Electrodes. *Sol. Energy Mater. Sol. Cells* **2012**, *98*, 118–123.
32. Guo, F.; Zhu, X.; Forberich, K.; Krantz, J.; Stubhan, T.; Salinas, M.; Halik, M.; Spallek, S.; Butz, B.; Spiecker, E.; *et al.* ITO-Free and Fully Solution-Processed Semitransparent Organic Solar Cells with High Fill Factors. *Adv. Energy Mater.* **2013**, *3*, 1062–1067.
33. De, S.; Higgins, T. M.; Lyons, P. E.; Doherty, E. M.; Nirmalraj, P. N.; Blau, W. J.; Boland, J. J.; Coleman, J. N. Silver Nanowire Networks as Flexible, Transparent, Conducting Films: Extremely High DC to Optical Conductivity Ratios. *ACS Nano* **2009**, *3*, 1767–1774.
34. Sun, Y.; Seo, J. H.; Takacs, C. J.; Seifter, J.; Heeger, A. J. Inverted Polymer Solar Cells Integrated with a Low-Temperature-Annealed Sol-Gel-Derived ZnO Film as an Electron Transport Layer. *Adv. Mater.* **2011**, *23*, 1679–1683.
35. Liu, J.; Jeong, H.; Liu, J.; Lee, K.; Park, J.-Y.; Ahn, Y. H.; Lee, S. Reduction of Functionalized Graphite Oxides by Trioctylphosphine in Non-Polar Organic Solvents. *Carbon* **2010**, *48*, 2282–2289.